MATERIALS SCIENCE

S. Siebentritt
U. Rau (Eds.)

Wide-Gap Chalcopyrites

Springer

Springer Series in
MATERIALS SCIENCE 86

Springer Series in

MATERIALS SCIENCE

The Springer Series in Materials Science covers the complete spectrum of materials physics, including fundamental principles, physical properties, materials theory and design. Recognizing the increasing importance of materials science in future device technologies, the book titles in this series reflect the state-of-the-art in understanding and controlling the structure and properties of all important classes of materials.

71 **Dissipative Phenomena in Condensed Matter**
Some Applications
By S. Dattagupta and S. Puri

72 **Predictive Simulation of Semiconductor Processing**
Status and Challenges
Editors: J. Dabrowski and E.R. Weber

73 **SiC Power Materials**
Devices and Applications
Editor: Z.C. Feng

74 **Plastic Deformation in Nanocrystalline Materials**
By M.Yu. Gutkin and I.A. Ovid'ko

75 **Wafer Bonding**
Applications and Technology
Editors: M. Alexe and U. Gösele

76 **Spirally Anisotropic Composites**
By G.E. Freger, V.N. Kestelman, and D.G. Freger

77 **Impurities Confined in Quantum Structures**
By P.O. Holtz and Q.X. Zhao

78 **Macromolecular Nanostructured Materials**
Editors: N. Ueyama and A. Harada

79 **Magnetism and Structure in Functional Materials**
Editors: A. Planes, L. Manõsa, and A. Saxena

80 **Ion Implantation and Synthesis of Materials**
By M. Nastasi and J.W. Mayer

81 **Metallopolymer Nanocomposites**
By A.D. Pomogailo and V.N. Kestelman

82 **Plastics for Corrosion Inhibition**
By V.A. Goldade, L.S. Pinchuk, A.V. Makarevich and V.N. Kestelman

83 **Spectroscopic Properties of Rare Earths in Optical Materials**
Editors: G. Liu and B. Jacquier

84 **Hartree–Fock–Slater Method for Materials Science**
The DV–X Alpha Method for Design and Characterization of Materials
Editors: H. Adachi, T. Mukoyama, and J. Kawai

85 **Lifetime Spectroscopy**
A Method of Defect Characterization in Silicon for Photovoltaic Applications
By S. Rein

86 **Wide-Gap Chalcopyrites**
Editors: S. Siebentritt and U. Rau

Volumes 20–70 are listed at the end of the book.

S. Siebentritt U. Rau (Eds.)

Wide-Gap Chalcopyrites

With 122 Figures (1 color) and 19 Tables

Springer

Dr. Susanne Siebentritt
Hahn-Meitner-Institut
Glienicker Str. 100, 14109 Berlin, Germany
Tel.: +49-30-8062 2442 fax: +49-30-8062 3199
E-mail: siebentritt@hmi.de
http://www.hmi.de/pubbin/vkart.pl?v=zky

Dr. Uwe Rau
Institute of Physical Electronics, University of Stuttgart
Pfaffenwaldring 47, 70569 Stuttgart, Germany
E-mail: uwe.rau@ipe.uni-stuttgart.de

ISSN 0933-033X

ISBN-10 3-540-24497-2 Springer Berlin Heidelberg New York

ISBN-13 978-3-540-24497-4 Springer Berlin Heidelberg New York

Library of Congress Control Number: 2005933718

Springer is a part of Springer Science+Business Media.
springer.com

Typesetting by the Authors and SPI Publisher Services using a Springer TEX macro package
Cover concept: eStudio Calamar Steinen
Cover production: *design & production* GmbH, Heidelberg

Printed on acid-free paper SPIN: 11382843 57/3141/SPI 5 4 3 2 1 0

Preface

Thin film solar modules are considered as the next generation of photovoltaics technology due to their higher cost reduction potential compared to conventional photovoltaic modules based on Si wafers. The cost advantages are dueto lower material and energy consumption, lower semiconductor quality requirements, smaller dimensions of thin films and integrated module production, leading to reduced manpower needs. Currently, thin film technologies are boosted additionally by the shortage in the supply of silicon. Thin film modules based on Cu-chalcopyrite absorbers represent the most advanced thin film technology with high efficiency laboratory cells and mass production starting 2006. These high-efficiency cells and commercial modules are based on absorbers with a bandgap around 1.1 eV. In recent years, the interest in chalcopyrite absorbers with wider bandgaps has considerably increased due to the efforts to increase solar cell effiencies by using absorbers closer to the solar spectrum optimum and by constructing a thin film tandem cell. To date, solar cells based on wide gap chalcopyrites have failed to reach the excellent performance levels of their low gap "cousins." The authors of this book have set out to investigate the reasons behind the inferior behaviour of the widegap chalcopyrite solar cells and to suggest solutions. The chapters in this book address the various aspects of this question in analysing the properties of wide-gap and low-gap materials. Most of the results presented here were obtained within a network research project funded by the German Ministry of Research and Education (BMBF): "Hochspannungsnetz" (high voltage network), which was aimed at characterising the defect and interface behaviour, as well as grain boundary properties in wide-gap chalcopyrites. The results were presented in two workshops in the fall of 2002 and 2003 in the village of Triberg in Black Forest and in Castle Reichenow near Berlin, respectively. In addition to the contributions of the project partners, the present compilation also contains papers from "external experts" invited to these workshops. We are especially grateful to D. Cohen, W. Mnch, J. van Vechten and W. Walukiewicz for joining the workshops and for their contributions to this book, highlighting important new aspects and original work that will be helpful for our ongoing research efforts.

Berlin and Stuttgart,
July 2005

Susanne Siebentritt
Uwe Rau

Contents

List of Contributors

M. Albrecht
Institute of Microcharacterisation
Department of Materials Science and Engineering
University of Erlangen-Nuremberg,
Cauerstr. 6
91058 Erlangen, Germany
albrecht@ww.uni-erlangen.de

G.H. Bauer
Faculty of Mathematics and Natural Sciences
Carl von Ossietzky University
26111 Oldenburg, Germany
g.h.bauer@uni-oldenburg.de

J.D. Cohen
Department of Physics
University of Oregon
Eugene, OR 97403, USA
dcohen@OREGON.UOREGON.EDU

G. Hanna
Institute of Physical Electronics (IPE)
University Stuttgart
Pfaffenwaldring 47
70569 Stuttgart, Germany
george.hanna@zsw-bw.de

J.T. Heath
Department of Physics
Linfield College
McMinnville
OR 97128, USA
jheath@linfield.edu

A. Klein
Surface Science Division
Institute of Materials Science
Darmstadt University of Technology
Petersenstrasse 23
D-64287 Darmstadt, Germany
aklein@surface.tu-darmstadt.de

R. Kniese
Zentrum für Sonnenenergie- und Wasserstoff-Forschung
Baden-Württemberg (ZSW)
Industriestr. 6
70565 Stuttgart, Germany
robert.kniese@zsw-bw.de

R. Menner
Zentrum für Sonnenenergie- und Wasserstoff-Forschung
Baden-Württemberg (ZSW)
Industriestr. 6
70565 Stuttgart, Germany
richard.menner@zsw-bw.de

W. Mönch
Department of Physics
Universität Duisburg-Essen
47048 Duisburg, Germany
w.moench@uni-duisburg.de

N. Ott
Institute of Microcharacterisation
Department of Materials Science
and Engineering
University of Erlangen-Nurember,
Cauerstr. 6,
91058 Erlangen, Germany
Niels.Ott@ww.uni-erlangen.de

M. Powalla
Zentrum für Sonnenenergie- und
Wasserstoff-Forschung
Baden-Württemberg (ZSW),
Industriestr. 6 70565 Stuttgart,
Germany
michael.powalla@zsw-bw.de

U. Rau
Institut für Physikalische Elektronik
(IPE)
University of Stuttgart,
Pfaffenwaldring 47
70569 Stuttgart, Germany
uwe.rau@ipe.uni-stuttgart.de

S. Sadewasser
Hahn-Meitner Institut
Glienicker Str. 100
14109 Berlin, Germany
sadewasser@hmi.de

T. Schulmeyer
Surface Science Division
Institute of Materials Science
Darmstadt University of Technology,
Petersenstrasse 23
D-64287 Darmstadt, Germany
tschulmeyer@
surface.tu-darmstadt.de

W.N. Shafarman
Institute of Energy Conversion
University of Delaware
Newark, DE 19716, USA
wns@udel.edu

S. Siebentritt
Hahn-Meitner-Institut
Glienicker Str. 100
14109 Berlin, Germany
siebentritt@hmi.de

U. Stein
Zentrum für Sonnenenergie- und
Wasserstoff-Forschung
Baden-Württemberg (ZSW),
Industriestr. 6 70565 Stuttgart,
Germany
ulrike.stein@zsw-bw.de

H.P. Strunk
Institute of Microcharacterisation
Department of Materials Science
and Engineering
University of Erlangen-Nuremberg,
Cauerstr. 6
91058 Erlangen, Germany
strunk@ww.uni-erlangen.de

M. Turcu
Institute of Physical Electronics
University of Stuttgart
Pfaffenwaldring 47
70569 Stuttgart, Germany
mircea.turcu@ipe.uni-stuttgart.de

J.A. Van Vechten
School of Electrical Engineering and
Computer Science
Oregon State University
Corvallis, OR 97331-3211, USA
JAvanvec@msn.com

G. Voorwinden
Zentrum für Sonnenenergie- und Wasserstoff-Forschung
Baden-Württemberg (ZSW),
Industriestr. 6 70565 Stuttgart,
Germany
georg.voorwinden@zsw-bw.de

W. Walukiewicz
Materials Sciences Division
Lawrence Berkeley National Laboratory
MS 2R0200, 1 Cyclotron Rd.
Berkeley, CA 94720-8197, USA
W_Walukiewicz@lbl.gov

1

Cu-Chalcopyrites – Unique Materials for Thin-Film Solar Cells

S. Siebentritt and U. Rau

Thin-film solar modules are considered as the next generation of photovoltaics technology due to their higher cost-reduction potential compared to conventional photovoltaic modules based on Si wafers. The cost advantages are due to lower material and energy consumption, lower semiconductor quality requirements, short distances in thin films, and integrated module production leading to reduced manpower needs. Currently, thin-film technologies are boosted additionally by shortage in the supply of Si.

Thin-film modules based on Cu-chalcopyrite absorbers [1] represent the most advanced thin-film technology with laboratory cells reaching efficiencies above 19% [2]. Modules of $Cu(In,Ga)(S,Se)_2$ solar cells are in the pilot production stage at several places worldwide and large modules have reached efficiencies above 13% [3] and output power of 80 W [4]. Mass production in Europe will start in 2006 [5].

The basic structure of these solar cells and the schematics of their band structure are shown in Fig. 1.1. The p/n junction is formed between the p-type chalcopyrite absorber and the window layer, usually a double layer of undoped-ZnO and Al-doped or Ga-doped ZnO. The quality of the heterojunction is greatly improved by the introduction of a CdS buffer layer; alternative Cd-free materials are under investigation [6].

The following list gives a brief account of potentially critical points of the $Cu(In,Ga)(S,Se)_2$ thin-film solar cell technology and the research that is aimed to solve these issues:

1. The photovoltaic junction is made by a heterocontact between two non-lattice matched materials, a situation that is potentially hazardous because of interface recombination via a high density of interface states. It is therefore desirable that the Fermi level at the absorber/buffer interface is above midgap, i.e., the interface should be type-inverted with respect to the absorber [7]. However, despite these type-inversion efficiencies, close to 20% would remain out of reach with this type of heterojunction, unless the special feature of a Cu-poor layer that forms spontaneously on the

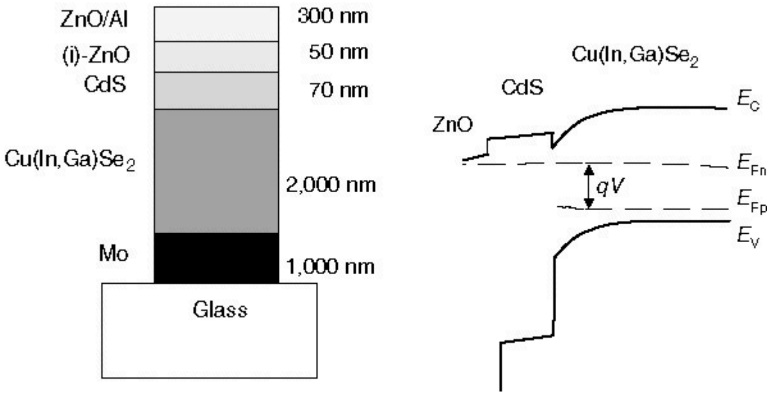

Fig. 1.1. Basic layer structure and energy-band diagram of a ZnO/CdS/$Cu(In,Ga)Se_2$ heterojunction solar cell under a bias with voltage V

surface of the absorber material would suppress interface recombination further as discussed in Chap. 6.

2. The Mo-coated glass serves as the substrate for the growth of the absorber material and, in addition, as the ohmic back contact for the completed solar cell. The glass substrate, usually ordinary soda-lime glass, is not a natural choice as part of a highly sophisticated electronic device, especially because of impurities, like alkali atoms contained in this material. Fortunately, introduction of Na from the soda-lime glass substrate contributes positively to the photovoltaic quality of the absorber material. Although the precise origin of this beneficial effect is not yet entirely understood, the presence of Na during absorber growth is mandatory for high-efficiency devices (for a detailed discussion see [8]). The suitability of Mo as the back contact of the device is also somewhat stunning as Mo on p-type $CuInSe_2$ is known to form a Schottky contact with a barrier height of 0.8 eV [9]. Hence, one would not guess that Mo does perform especially well as an ohmic back contact for a $CuInSe_2$ solar cell. Fortunately, it turns out that a $MoSe_2$ film of thickness of few ten nm forms on top of the Mo layer during absorber growth, thus enabling excellent ohmic properties of the back contact [10].
3. The $Cu(In,Ga)(S,Se)_2$ absorber is a polycrystalline material with a grain size between few hundred nm and few µm. Thus, the grain size barely matches the film thickness and is more than four orders of magnitude smaller than the size of the grains in polycrystalline silicon that delivers about the same solar cell efficiencies as the small-grained $Cu(In,Ga)(S,Se)_2$. Therefore, the electronic activity of grain boundaries and other extended defects must be extraordinarily low. Due to their benign manner, these defects seemed unimportant and only recently has attention been focused

on them. Possibly, the peculiar phase and defect behavior of the Cu-chalcopyrites material also influences the optoelectronic properties of grain boundaries as it does for the surfaces. The nature of grain boundaries is dealt with in Chaps. 9 and 10 .

4. The ZnO/CdS/Cu(In,Ga)(S,Se)$_2$/Mo heterojunction solar cell is a very complicated system, with at least 11 chemical elements known to contribute actively to the electronic quality of the device. Because of the large variety of chemical reactions among these elements, chemical stability, especially at material interfaces, becomes an extremely critical question (for a review of the chemical stability, see [11]). Up to this point, we have dealt with the complex properties of the external and internal *interfaces* of the layer system shown in Fig. 1.1. Concentrating on the *bulk* properties of Cu-chalcopyrite absorbers, we have to consider the defect physics of a ternary compound.
5. A ternary compound (like $CuInSe_2$) already possesses 12 possible *intrinsic defects.* Therefore, even without considering the effects of In/Ga or S/Se alloying, we see that we are already dealing with a very complex defect chemistry. In addition, most of these intrinsic defects have very low defect formation energies, below 1 eV [12], which is very small compared to any other compound or elemental semiconductor. Moreover, the formation energy of *defect complexes* of the structure ($2\,V_{Cu^-}$–$In_{Cu^{2+}}$) becomes negative in Cu-poor materials. The fact that this defect complex is electrically inactive is one of the reasons that make $CuInSe_2$ a photovoltaic-attractive material. The occurrence of several Cu-poor phases, e.g., $CuIn_3Se_5$ and $CuIn_5Se_8$, is explained by the regular ordering of these complexes. The electronically beneficial nature of these phases in solar cells results from the fact that they have a band-gap energy larger than the stoichiometric chalcopyrite. The formation of a surface layer with reduced Cu concentration at the surface of Cu-poor films (see point 1 and [13, 14]) plays a critical role in the interface formation as is discussed in Chaps. 6 and 11.
6. The ease with which defects are formed in chalcopyrite materials also leads to an unusually large existence region of the chalcopyrite phase, which extends far into the Cu-poor region [15, 16]. On the other hand, Cu excess is not incorporated into the chalcopyrite; it forms an additional Cu–Se phase at the surface.
7. The low defect formation energies are also the basis for the unusual stabilization of the polar surfaces. In other compound semiconductors like ZnSe and GaAs, the non-polar surfaces are the stable ones, while in chalcopyrites it is the (112) surfaces that are stable [17] – these correspond to the (111) surfaces in the cubic lattice. This can be explained by the removal of the surface dipole by defect formation [18,19], leading to Cu-poor surfaces.
8. Maybe the major effect of the low defect formation energies is the fact that the Cu-chalcopyrites are doped by their native defects. No impurity doping is used to obtain the p-type nature of the solar cell absorbers.

Up to date, there exists no reliable information on the chemical nature of the defects. Nevertheless, some trends are observed: $CuInSe_2$ tends to be p-type under Se-excess or Cu-excess conditions and n-type under Se-deficient conditions [20,21]. On the other hand, $CuGaSe_2$, which shows the same shallow defects as $CuInSe_2$ (discussed in Chap. 7), is always p-type under any stoichiometric deviation. The difficulty in obtaining chemical information on the involved defects is directly based on the ternary nature of these compounds. In binary materials, defect-chemical information can be obtained from annealing experiments controlling the concentration of one of the compounds. For ternary compounds this would only be possible by controlling the concentration of two of the three compounds [22], which is experimentally extremely difficult. Therefore, most annealing experiments are done controlling only one component, rendering their results very unreliable.

At this point, the reader is reminded that all beneficial circumstances discussed earlier are strictly valid only for a narrow composition range of the $Cu(In,Ga)(S,Se)_2$ system, namely those alloys with low Ga and S contents. Consequently, record-efficiency cells have a band gap energy, E_g of about 1.1–1.15 eV. However, the entire alloy system allows the control of the band gap between 1.05 eV($CuInSe_2$) and 2.5 eV ($CuGaS_2$). Therefore, a considerable amount of research and technological development directs towards those compositions that have a wider band gap than the up-to-now optimum material. This is motivated by the following reasons [23, 24]:

1. The band gap energy $E_g \approx 1.1$ eV is below the optimum match to the solar spectrum. Therefore, higher efficiencies are expected from wider gap alloys as long as the recombination and transport properties of the wide-gap devices correspond to those of the best low-gap devices.
2. The lower current densities in wide-gap devices lead to lower resistive losses, thus allowing for wider cells within a solar module and thus reducing the number of necessary scribes for monolithic integration of the cells into a module. Also, the thickness of front and back electrodes can be reduced.
3. Wide-gap solar cells are expected to have a better temperature coefficient and, therefore, to perform better under real-world operating conditions than low-gap cells.
4. Wide-gap absorbers are better suited for space applications since the degradation of the open circuit voltage (V_{OC}) due to radiation is less critical in devices with a high V_{OC} than in low-gap devices with a corresponding low V_{OC} [25].
5. The free electron absorption in highly conducting ZnO window materials is not as critical for wide-gap materials as for low-gap materials, where the absorption of infrared light in ZnO overlaps with the absorption of the absorber material.

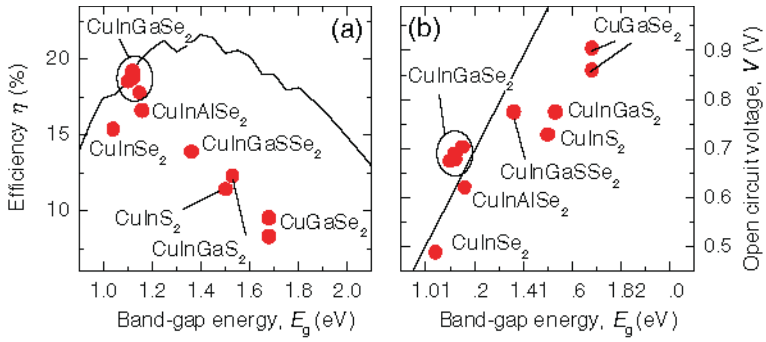

Fig. 1.2. (**a**) Highest published conversion efficiencies of solar cells from $CuInSe_2$ [4], Cu(In,Ga)Se_2 [2, 29, 30], Cu(In,Al)Se_2 [31], Cu(In,Ga)(S,Se)$_2$ [32], $CuInS_2$ [33], Cu(In,Ga)S_2 [34], and $CuGaSe_2$ [27,35] as a function of the band-gap energies E_g of the absorber materials. (**b**) Open circuit voltages of the cells shown in (**a**). The *solid lines* in (**a**) and (**b**) stem from an extrapolation of the recombination properties of the best Cu(In,Ga)Se_2 solar cells toward higher and lower E_gs

6. The wide range of band gap energies (E_g) of the Cu(In,Ga)(S,Se)$_2$ alloy system embraces combinations of E_g that in principle allow us to build Cu-chalcopyrite based tandem solar cells [26].

Thus, research and development on wide-gap chalcopyrite is an attractive issue because of the technological flexibility that is provided by mastering an alloy system with band gap energies matching the entire solar spectrum.

Unfortunately, all attempts to achieve efficiencies in the range of 17–20% by using wide-gap chalcopyrites have failed so far. For example, $CuGaSe_2$ solar cells have not reached the 10% efficiency level yet [27]; only by the addition of a small amount of In an efficiency of 10.5% was reached [28]. Figure 1.2a gives an overview of the power conversion efficiencies that have been obtained with different Cu-chalcopyrite alloys featuring a sharp drop when using band gap energies in excess of 1.2 eV. The reason for the low efficiencies lies in the fact that the open circuit voltages of these devices do not correspond to those values that are expected from their larger band-gap energies (Fig. 1.2b).

Up to now, research and development have not identified the physical origin of the relatively poor photovoltaic performance of the wide-gap chalcopyrites. Obviously, the unique solutions and features found while developing the low-gap absorbers are not directly suitable for their wide-gap counterparts. In addition, critical issues (see the eight-point list discussed earlier) have been solved and understood for the low-gap alloys after a long research effort. For their wide-gap counterparts, we should be aware that we may not necessarily benefit again from the goodwill of nature as much as in the low-gap alloys.

Only slightly deteriorated interface properties at the frontelectrode and back electrode, only slightly altered grain boundary properties and only comparatively small changes in the defect chemistry, may sum up to the considerably degraded performance. Thus, all ingredients that are obviously necessary to achieve the excellent photovoltaic performance of the low-gap chalcopyrites must be critically checked for their applicability to wide-gap alloys.

The following chapters address these different aspects in analyzing the properties of wide-gap and low-gap materials. Most of the results presented here were obtained in a network research project funded by the German Ministry of Research and Education (BMBF) – “Hochspannungsnetz” (high-voltage network), which was aimed at characterizing the defect and interface behavior as well as grain boundary properties in wide-gap chalcopyrites. The results were presented in two workshops in the fall of 2002 and 2003 in the village of Triberg in Black Forest and in castle Reichenow near Berlin, respectively. In addition to the contributions of the project partners, the present compilation also contains papers from “external experts” invited to these workshops. We are especially grateful to D. Cohen, W. Mönch, J. van Vechten, and W. Walukiewicz for joining the workshops and for their contributions to this book, highlighting important new aspects and original work that will be helpful for our ongoing research efforts.

References

1. Shay, J.L., Wernick, J.H.: Ternary Chalcopyrite Semiconductors: Growth, Electronic Properties and Application. Pergamon Press, Oxford (1975)
2. Ramanathan, K., Contreras, M.A., Perkins, C.L., Asher, S., Hasoon, F.S., Keane, J., Young, D., Romero, M., Metzger, W., Noufi, R., Ward, J., Duda, A.: Properties of 19.2% efficiency ZnO/CdS/$CuInGaSe_2$ thin-film solar cells. Prog. Photovolt. Res. Appl. 11, 225–230 (2003)
3. Probst, V., Stetter, W., Palm, J., Toelle, R., Visbeck, S., Calwer, H., Niesen, T., Vogt, H., Hernández, O., Wendl, M., Karg, F.H.: CIGSSE module pilot processing: from fundamental investigations to advanced performance. In: Kurokawa, K., Kazmerski, L.L., McNelis, B., Yamaguchi, M., Wronski, C., Sinke, W.C. (eds.) Proceedings of the 3rd World Conference on Photovoltaic Solar Energy Conversion, pp. 329–334. Arisumi Printing Inc., Osaka, Japan (2003)
4. Powalla, M., Dimmler, B.: New developments in CIGS thin-film solar cell technology. In: Kurokawa, K., Kazmerski, L.L., McNelis, B., Yamaguchi, M., Wronski, C., Sinke, W.C. (eds.) Proceedings of the 3rd World Conference on Photovoltaic Solar Energy Conversion, pp. 313–318. Arisumi Printing Inc., Osaka, Japan (2003)
5. Powalla, M., Dimmler, B., Schäffler, R., Voorwinden, G., Stein, U., Mohring, H.-D., Kessler, F., Hariskos, D.: CIGS solar modules – progress in pilot production, new developments and applications. In: Ossenbrinck, H.A. (ed.) Proceedings of the 19th European Photovoltaic Solar Energy Conference. pp. 1663–1668. JRC, Ispra, Italy (2004)
6. Siebentritt, S.: Alternative buffers for chalcopyrite solar cells. Solar Energy 77, 767–775 (2004)
7. Klenk, R.: Characterization and modelling of chalcopyrite solar cells. Thin Solid Films 387, 135–140 (2001)

8. Rau, U., Schock, H.W.: Electronic properties of Cu(In,Ga)Se_2 heterojunctio solar cells — recent achievements, current understanding, and future challenges. Appl. Phys. A 69, 131–147 (1999)
9. Jaegermann, W., Löher, T., Pettenkofer, C.: Surface properties of chalcopyrite semiconductors. Cryst. Res. Technol. 31, 273–280 (1996)
10. Nishiwaki, S., Kohara, N., Negami, T., Wada, T.: $MoSe_2$ layer formation at Cu(In,Ga)Se_2/Mo interfaces in high efficiency $Cu(In_{1-x}Ga_x)Se_2$ solar cells. Jpn. J. Appl. Phys. (Part 2) 37, 71–73 (1998)
11. Guillemoles, J.F., Kronik, L., Cahen, D., Rau, U., Jasenek, A., Schock, H.W.: Stability issues of Cu(In,Ga)Se_2-based solar cells. J. Phys. Chem. B 104, 4849–4862 (2000)
12. Zhang, S.B., Wei, S.-H., Zunger, A., Katayama-Yoshida, H.: Defect physics of the $CuInSe_2$ chalcopyrite semiconductor. Phys. Rev. (B) 57, 9642–9656 (1998)
13. Schmid, D., Ruckh, M., Grunwald, F., Schock, H.W.: Chalcopyrite/defect chalcopyrite heterojunctions on the basis of $CuInSe_2$. J. Appl. Phys. 73, 2902–2909 (1993)
14. Schmid, D., Ruckh, M., Schock, H.W.: Photoemission studies on Cu(In,Ga)Se_2 thin films and related binary selenides. Appl. Surf. Sci. 103, 409–429 (1996)
15. Fearheiley, M.: The phase relations in the Cu, In, Se system and the growth of $CuInSe_2$ single crystals. Solar Cells 16, 91–100 (1986)
16. Mikkelsen, J.C. Jr.: Ternary phase relations of the chalcopyrite compound $CuGaSe_2$. J. Electron. Mater. 10, 541–558 (1981)
17. Liao, D., Rockett, A.: Epitaxial growth of Cu(In,Ga)Se_2 on GaAs(110). J. Appl. Phys. 91, 1978–1983 (2002)
18. Jaffe, J.E., Zunger, A.: Defect-induced nonpolar-to-polar transition at the surface of chalcopyrite semiconductors. Phys. Rev. (B) 64, 241301–241304 (2001)
19. Zhang, S.B., Wei, S.-H.: Reconstruction and energetics of the polar (112) and (−1−1−2) versus the nonpolar (220) surfaces of $CuInSe_2$. Phys. Rev. (B) 65, 081402-1–081401-4 (2002)
20. Tell, B., Shay, J.L., Kasper, H.M.: Room-temperature electrical properties of ten I–III–VI2 semiconductors. J. Appl. Phys. 43, 2469 (1972)
21. Noufi, R., Axton, R., Herrington, C., Deb, S.K.: Electronic properties vs composition of thin films of $CuInSe_2$. Appl. Phys. Lett. 45, 668–670 (1984)
22. Bardeleben, H.J.V.: The chemistry of structural defects in $CuInSe_2$. Solar Cells 16, 381–390 (1986)
23. Siebentritt, S.: Wide gap chalcopyrites: material properties and solar cells. Thin Solid Films 403–404, 1–8 (2002)
24. Rau, U.: Electronic properties of wide-gap Cu(In,Ga)(S,Se)$_2$ solar cells. In: Kurokawa, K., Kazmerski, L.L., McNelis, B., Yamaguchi, M., Wronski, C., Sinke, W.C. (eds.) Proceedings of the 3rd World Conference on Photovoltaic Solar Energy Conversion, pp. 2847–2852. Arisumi Printing Inc., Osaka, Japan (2003)
25. Jasenek, A., Hahn, T., Schmidt, M., Weinert, K., Wimbor, M., Hanna, G., Orgassa, K., Hartmann, M., Schock, H.W., Rau, U., Werner, J.H., Schattat, B., Kraft, S., Schmid, K.H., Bolse, W., Roche, G.L., Robben, A., Bogus, K.: Stability of Cu(In,Ga)Se_2 thin film solar cells under 1 MeV electron radiation. In: Proceedings of the 16th European Photovoltaic Solar Energy Conference and Exhibition, pp. 982–985, 2000

26. Nishiwaki, S., Siebentritt, S., Walk, P., Lux-Steiner, M.C.: A stacked chalcopyrite thin-film tandem solar cell with 1.2 V open-circuit voltage. Prog. Photovolt. Res. Appl. 11, 243–248 (2003)
27. Young, D.L., Keane, J., Duda, A., AbuShama, J.A.M., Perkins, C.L., Romero, M., Noufi, R.: Improved performance in ZnO/CdS/$CuGaSe_2$ thin-film solar cells. Prog. Photovolt. Res. Appl. 11, 535–541 (2003)
28. Symco-Davies, M., Noufi, R., Coutts, T.J.: Progress in high performance PV-polycrystalline thin film tandem cells. In: Hoffmann, W., Bal, J.-L., Ossenbrinck, H.A. (eds.) Proceedings of the 19th European Photovoltaic Solar Energy Conference. pp. 1651–1656. JRC, Ispra, Italy (2004)
29. Orgassa, K., Nguyen, Q., Kötschau, I.M., Rau, U., Schock, H.W., Werner, J.H.: Optimized reflection of CdS/ZnO window layers in Cu(In,Ga)Se_2 thin-film solar cells. In: McNelis, B., Palz, W., Ossenbrinck, H.A., Helm, P. (eds.) Proceedings of the 17th European Photovoltaic Solar Energy Conference, WIP-Munich Germany, pp. 1039–1042, 2002
30. Negami, T., Hashimoto, Y., Nishiwaki, S.: Cu(In,Ga)Se_2 thin-film solar cells with an efficiency of 18%. Sol. Energy Mater. Sol. Cells 67, 331–335 (2001)
31. Marsillac, S., Paulson, P.D., Haimbodi, M.W., Birkmire, R.W., Shafarman, W.N.: High-efficiency solar cells based on Cu(InAl)Se_2 thin films. Appl. Phys. Lett. 81, 1350–1352 (2002)
32. Friedlmeier, T.M., Schock, H.W.: Improved voltages and efficiencies in Cu(In,Ga)$(S,Se)_2$ solar cells. In: Schmid, J., Ossenbrink, H.A., Helm, P., Ehmann, H., Dunlop, E.D. (eds.) Proceedings of the 2nd World Conference on Photovoltaic Solar Energy Conversion. European Commission, Luxembourg, pp. 1117–1120 (1998)
33. Siemer, K., Klaer, J., Luck, I., Bruns, J., Klenk, R., Braunig, D.: Efficient $CuInS_2$ solar cells from a rapid thermal process (RTP). Sol. Energy Mater. Sol. Cells 67, 159–166 (2001)
34. Kaigawa, R., Neisser, A., Klenk, R., Lux-Steiner, M.Ch.: Improved performance of thin film solar cells based on Cu(In,Ga)S_2. Thin Solid Films 415, 266–271 (2002)
35. Nadenau, V., Hariskos, D., Schock, H.W.: $CuGaSe_2$ thin film solar cells with improved performance. In: Ossenbrink, H.A., Helm, P., Ehmann, H. (eds.) Proceedings of the 14th European Photovoltaic Solar Energy Conference, Stephens, Bedford, pp. 1250–1253, 1997

2

Band-Structure Lineup at I–III–VI_2 Schottky Contacts and Heterostructures

W. Mönch

2.1 Introduction

As with all other semiconductor devices, the band-structure lineup in chalcopyrite solar cells also determines their electronic properties. For improvements of the fabrication processes and the design of new device concepts, it is desirable to have some insight into the physical mechanisms that determine the barrier heights and the band-edge offsets of the I–III–VI_2 Schottky contacts and heterostructures, respectively. As this chapter will demonstrate, the I–III–VI_2 chalcopyrites behave quite the same as all other semiconductors, in that their Schottky barrier heights and heterostructure-band offsets are also explained by the continuum of interface-induced gap states(IFIGS).

The rectifying properties of metal–semiconductor contacts were discovered by Braun [1]; and Schottky [2] explained them by a depletion layer on their semiconductor side. Schottky's explanation shifted the focus to the physical mechanisms, which determine the barrier heights of metal–semiconductor contacts, i.e., the energy position of the Fermi level, relative to the band-edge of the majority charge carriers at the interface. The early Schottky–Mott rule [3, 4] proposed the n-type (p-type) barrier height $\Phi_{\mathrm{Bn,p}}$ of a metal–semiconductor contact to equal the difference between the work function Φ_{m} of the metal and the electron affinity (ionization energy) of the semiconductor in contact. However, the slope parameter $S_{\Phi} = -\mathrm{d}\Phi_{\mathrm{Bp}}/\mathrm{d}\Phi_{\mathrm{m}}$ of metal–selenium rectifiers turned out to be much smaller than unity, the value predicted by the Schottky–Mott rule. Schottky [4] consequently concluded the failure of this simple rule in 1940. But most surprisingly, some groups still believe it to be valid for ideal Schottky contacts.

Bardeen [5] proposed electronic interface states to exist in the semiconductor band-gap at Schottky contacts. The charge absorbed in these interface states and the depletion layer then compensates the charge on the metal side of Schottky contacts and, as a consequence, the slope parameter S_{Φ} will become smaller than unity, the value predicted by the Schottky–Mott rule. Considering the quantum-mechanical tunnel effect at metal–semiconductor interfaces, Heine [6] noted that for energies in the semiconductor band-gap the volume states of the metal have tails in the semiconductor. Tejedor and Flores [7] applied this idea to semiconductor heterostructures, where for energies in the band-edge discontinuities the volume states of one semiconductor tunnel into the other one.

The continua of these IFIGS are an *intrinsic* property of the semiconductors and they are the *fundamental* mechanism that determines both the barrier heights of Schottky contacts and the band offsets of semiconductor heterostructures. The IFIGS derive from the valence-band and conduction-band states of the semiconductor. The sign and the amount of the net charge in the IFIGS depend on the Fermi-level position relative to their branch point where their character changes from predominantly valence-band-like or donor-like to mostly conduction-band-like or acceptor-like. Hence, the IFIGS give rise to intrinsic interface dipoles. Both Schottky barrier heights and band offsets in heterostructures thus divide into a zero-charge-transfer term and a dipole contribution.

From a more chemical point of view, these interface dipoles are attributed to the partial ionic character of the covalent bonds between interface atoms. In generalizing Pauling's electronegativity concept [8], the difference of the electronegativities of the atoms involved in the interfacial bonds then describes the charge transfer at semiconductor interfaces. In combining the physical IFIGS and the chemical electronegativity concept, the dipole contributions of the Schottky barrier heights as well as the heterostructure-band offsets vary proportional to the difference of the electronegativities of the metal and the semiconductor and of the two semiconductors that are in contact, respectively.

Theoreticians appreciated Heine's IFIGS concept at once, but the experimentalists adopted it very slowly. One of the reasons was that the theoretical IFIGS lines marked upper limits of the barrier heights of *real* Schottky contacts only [9, 10]. Schmitsdorf et al. [11] resolved this dilemma. They found a linear decrease of the effective barrier heights with increasing ideality factors of their Ag/n-Si(1 1 1) diodes. Such a behavior is observed with all Schottky contacts investigated so far. Schmitsdorf et al. attributed this correlation to patches of decreased barrier heights and lateral dimensions smaller than the depletion-layer width. Consequently, they extrapolated their plots of effective barrier heights vs the ideality factors to the ideality factor that is determined by the image force or Schottky effect [12] only and, in this way, obtained the barrier heights of laterally homogenous contacts.

The barrier heights of laterally uniform contacts may also be determined by applying ballistic electron emission microscopy (BEEM) and internal photoemission yield spectroscopy (IPEYS). The I/V, BEEM, and IPEYS data agree within the margins of experimental error. Mönch [13–15] plotted the barrier heights of laterally homogenous Si, GaN, GaP, GaAs, ZnSe, and 3C-SiC, 6H-SiC, and 4H-SiC Schottky contacts vs the difference of the metal and the semiconductor electronegativities. He found excellent agreement of the experimental data with the predictions of the IFIGS and electronegativity theory.

The IFIGS dipole term or, in other words, the difference between the metal and semiconductor electronegativities determines the dependence of the barrier heights of Schottky contacts with different metals on one and the same semiconductor. The electronegativities of the semiconductors are equal to within 10% since the elements that constitute the semiconductors are all placed in the middle of the Periodic Table of the Elements. Hence, the IFIGS dipole term of semiconductor heterostructures will be small and may be neglected [16]. The valence-band offsets of lattice-matched and non-polar as well as metamorphic heterostructures should thus equal the difference of the branch-point energies of the semiconductors in contact. The experimentally observed valence-band offsets of semiconductor heterostructures excellently confirm this prediction of the IFIGS-and-electronegativity theory [15].

This chapter is organized such that first a database of experimental barrier heights and valence-band offsets of I–III–VI_2 Schottky contacts and heterostructures, respectively, is compiled. Section 2.3 describes the IFIGS-and-electronegativity theory of the band-structure lineup at semiconductor interfaces. Section 2.4 is devoted to a comparison of experimental and theoretical data.

2.2 Experimental I–III–VI_2 Database

2.2.1 Barrier Heights of I–III–VI_2 Schottky Contacts

The barrier heights of Schottky contacts are generally determined from their current–voltage and capacitance–voltage characteristics (I/V, C/V) and by applying IPEYS and BEEM. No BEEM studies of I–III–VI_2 Schottky contacts have been published so far. Therefore, the evaluation of I/V, C/V and IPEYS characteristics will be outlined only briefly.[1]

I/V Characteristics

The current transport in real Schottky contacts occurs via thermionic emission provided the doping level of the semiconductor is not too high. The current–voltage characteristics may then be written as (see [15] for example):

$$I = AA_R^*T^2 \exp(-\Phi_{Bn}^{eff}/k_BT)\exp(e_0V_c/nk_BT)[1-\exp(-e_0V_c/k_BT)], \quad (2.1)$$

where A is the diode area, A_R^* is the effective Richardson constant of the semiconductor, and k_B, T, and e_0 are Boltzmann's constant, the temperature, and the electronic charge, respectively. The externally applied bias V_a divides up

[1]For a more detailed description of these techniques see [15].

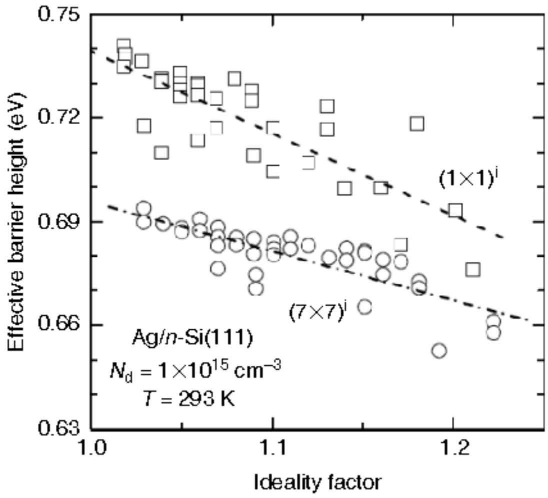

Fig. 2.1. Effective barrier heights vs ideality factors determined from I/V curves of Ag/n-Si(1 1 1)-$(7\times7)^i$ and Ag/n-Si(1 1 1)-$(1\times1)^i$ contacts at room temperature. The *dashed and dash-dotted lines* are linear least-squares fits to the data. From Schmitsdorf et al. [11]

into a voltage drop V_c across the depletion layer of the Schottky contact and an IR drop at the series resistance R_s of the diode, i.e., $V_\mathrm{c} = V_\mathrm{a} - IR_\mathrm{s}$. For *ideal*, i.e., intimate, abrupt, defect-free, and above all, laterally homogenous Schottky contacts, the effective zero-bias barrier height $\Phi^\mathrm{eff}_\mathrm{Bn}$ equals the difference $\Phi^\mathrm{hom}_\mathrm{Bn} - \delta\Phi^0_\mathrm{if}$ of the homogenous barrier height and the zero-bias image-force lowering. The ideality factor n describes the voltage dependence of the barrier height. For *real* diodes the ideality factors n are generally larger than the ideality factor n_if, which is determined by the image-force effect only.

The effective barrier heights and the ideality factors of real Schottky diodes fabricated under experimentally identical conditions differ from one specimen to another. However, the variations of both quantities are correlated. As an example, Fig. 2.1 displays effective barrier heights plotted vs the ideality factors of two sets of Ag/n-Si(1 1 1) contacts at room temperature. They differ in that the Si interface layers are either $(1\times1)^i$-unreconstructed or exhibit a $(7\times7)^i$ reconstruction. Both data sets reveal a pronounced correlation between the effective barrier heights and the ideality factors in that the effective barrier heights become smaller as the ideality factors increase. The dashed and dash-dotted lines are linear least-squares fits to the data. The dependence of the effective barrier heights on the ideality factors may thus be written as [11]

$$\Phi^\mathrm{eff}_\mathrm{Bn} = \Phi^\mathrm{nif}_\mathrm{Bn} - \varphi_\mathrm{p}(n - n_\mathrm{if}), \tag{2.2}$$

where $\Phi^\mathrm{nif}_\mathrm{Bn}$ is the barrier height at the ideality factor n_if, which is determined by the image-force effect only. The diodes with $(1\times1)^i$-unreconstructed interfaces have a larger $\Phi_{\mathrm{Bn}}^{\mathrm{nif}}$ value than the contacts with $(7\times7)^i$-reconstructed interfaces.

Several conclusions may be immediately drawn from relation (2.2). First, the correlation between effective barrier heights and ideality factors demonstrates the existence of more than just one physical mechanism that determines the barrier heights of *real* Schottky contacts. Second, the extrapolation of $\Phi_{\mathrm{Bn}}^{\mathrm{eff}}$ vs n curves to n_{if}, the ideality factor controlled by the image-force effect only, leaves all effects out of consideration, which causes a larger bias dependence of the barrier height than the image-force effect itself. Third, the extrapolated barrier heights $\Phi_{\mathrm{Bn}}^{\mathrm{nif}}$ are equal to the zero-bias barrier height $\Phi_{\mathrm{Bn}}^{0} = \Phi_{\mathrm{Bn}}^{\mathrm{hom}} - \delta\Phi_{\mathrm{if}}^{0}$. The superscript hom indicates that the barrier heights are laterally uniform or homogenous.

The homogenous barrier heights obtained from extrapolations of $\Phi_{\mathrm{B}}^{\mathrm{eff}}$ vs n curves to n_{if}, the ideality factor controlled by the image-force effect only, are not necessarily the barrier heights of the corresponding *ideal* contacts. This is illustrated by the two data sets displayed in Fig. 2.1. The corresponding diodes differ in their interface structures, $(1\times1)^i$-unreconstructed and $(7\times7)^i$-reconstructed. Generally, structural rearrangements are connected with a redistribution of the valence charge. The bonds in perfectly ordered bulk silicon (the example considered here) are purely covalent and, therefore, reconstructions are accompanied by $\mathrm{Si}^{-\Delta q}$–$\mathrm{Si}^{+\Delta q}$ dipoles. In a simple point-charge model, reconstruction-displaced and then charged-silicon interface atoms may be treated in the same way as foreign atoms at interfaces: The electronegativities of the foreign and the semiconductor-substrate atoms generally differ so that they induce interfacial dipoles. Depending on their orientation, such extrinsic dipole layers increase or lower the barrier heights (see [15] for example).

Patches of reduced barrier height with lateral dimensions smaller than the depletion layer width, which are embedded in large areas of laterally homogenous barrier height is the only model known that explains a lowering of effective barrier heights with increasing ideality factors. In their phenomenological studies of such patchy Schottky contacts, Freeouf et al. [17, 18] found the potential distribution to show a saddle point *in front* of such nm-size patches of reduced barrier height. Figure 2.2 explains this behavior. For example, in front of circular patches, the barrier height right at the saddle point is lowered with respect to the laterally homogenous barrier height of the embedding area [19] by

$$\delta\Phi_{\pi}^{\mathrm{sad}} = \gamma_{\pi}\left[(\Phi_{\mathrm{Bn}}^{\mathrm{hom}} - W_{\mathrm{n}} - e_0 V_{\mathrm{c}})k_{\mathrm{B}}T/L_{\mathrm{D}}^2\right]^{1/3}, \tag{2.3}$$

where $W_{\mathrm{n}} = W_{\mathrm{cb}} - W_{\mathrm{F}}$ and L_{D} are the energy distances from the Fermi level to the conduction-band edge in the bulk and the Debye length of the semiconductor, respectively. The saddle-point barrier height is determined by the patch parameter